DFT and electrochemical study on some iron(III) complexes with 2-hydroxybenzophenones

*Emmie Chiyindiko,[1] Ernst H.G. Langner[1] and Jeanet Conradie[1,2,]**

1 Department of Chemistry, University of the Free State, P.O. Box 339, 9300 Bloemfontein, South Africa

2 Department of Chemistry, UiT - The Arctic University of Norway, N-9037 Tromsø, Norway

Contact author details:

Name: Jeanet Conradie, Tel: ++27-51-4012194, email: conradj@ufs.ac.za

Research highlights

- Synthesis of iron(III) complexes containing 2-hydroxybenzophenones
- Electrochemical investigation of iron(III) complexes containing 2-hydroxybenzophenones
- DFT investigations to shed light on the observed Fe(III/II) reduction
- Comparison of electrochemical behaviour of ligands and their iron(III) and copper(II) complexes

Keywords

iron(III), 2-hydroxybenzophenone; DFT; redox potential

SYNOPSIS TOC

$$[Fe^{III}(HBP)_3] \underset{-e^-}{\overset{+e^-}{\rightleftharpoons}} [Fe^{II}(HBP)_3]^-$$

$$[Cu^{II}(HBP)_2] \xrightarrow{+e^-} [Cu^{I}(HBP)_2]^-$$

$$HBP \xrightarrow{+e^-} HBP^{\bullet -}$$

SYNOPSIS TEXT

Density functional theory calculations and cyclic voltammetry of tris(2-hydroxybenzophenone)iron(III) complexes showed that their reduction is metal-based.

Abstract

The synthesis, identification and electrochemical behaviour iron(III) complexes containing different 2-hydroxybenzophenone ligands are reported. The first reduction of the tris(2-hydroxybenzophenone)iron(III) complexes follow the same trend as that of the free, uncoordinated ligands and bis(2-hydroxybenzophenone)copper(II) complexes. The first reduction of the iron(III) complexes occur at a potential ca 1 V more positive than the reduction of the free ligands, but within 0.06 V of the reduction of bis(2-hydroxybenzophenone)copper(II) complexes. DFT calculations showed that [Fe(HBP)$_3$] (where HBP = 2-hydroxybenzophenone) is high-spin. Calculations further showed that tris(2-hydroxybenzophenone)iron(III) complexes can exist as both the *fac* and *mer* isomers. DFT calculations further showed that the first reduction of the tris(2-hydroxybenzophenone)iron(III) complexes is iron based, while further reductions are ligand based.

1 Introduction

Metal atoms, especially iron, are present at the active catalytic centre in almost a third of all known enzymes [1]. Iron(III) shows biochemical activity due to its capacity to both donate and accept electrons. Consequently it plays a crucial role in the metabolic processes of biological systems as a vital element [2–4]. Several iron(III) catalysts are used as starting material for a wide range of chemicals and intermediates in renewable biodiesel [5]. In response to the defining climate change crisis, industries are moving to more cost-effective and eco-friendly manufacturing and simultaneously reducing usage and production of substances hazardous to the environment and human health, an approach termed “green chemistry”. In the last decade, iron catalysts have received much attention due to their nontoxic, abundant, and inexpensive qualities [6].

In all catalytic processes the redox state of the catalyst is important. Metal complexes with variable oxidation states are likely candidates as redox shuttles, because of a shift in their redox potentials with varying ligands. We have recently reported on the redox properties of a series of bis(2-hydroxybenzophenone)copper(II) [7] and tris(2-hydroxybenzophenone)manganese(III) [8] complexes, showing that the copper(II/I) reduction is irreversible while the Mn(III/II) reduction is quasi reversible. We were interested to investigate the redox behaviour of related iron complexes; if

they have irreversible, quasi reversible or reversible redox behaviour, and how 2-hydroxybenzophenone ligands influence the observed redox behaviour of the tris(2-hydroxybenzophenone)iron(III) complexes. In this research, we provide an experimental electrochemical and a theoretical computational chemistry study of tris(2-hydroxybenzophenone)iron(III) complexes shown in Scheme 1 (a). The redox behaviour of the tris(2-hydroxybenzophenone)iron(III) are compared to the redox behaviour of the free, uncoordinated ligands and the related bis(2-hydroxybenzophenone)copper(II) complexes (Scheme 1). The tris(2-hydroxybenzophenone)iron complexes can exist in two structural isomeric forms, namely the *fac* and *mer* isomers, according to the arrangement of the three 2-hydroxybenzophenone ligands around the iron(III) metal centre. The experimental findings in this study are further supported by a density functional theory study (DFT) of the spin state, geometry and frontier orbitals of these iron complexes.

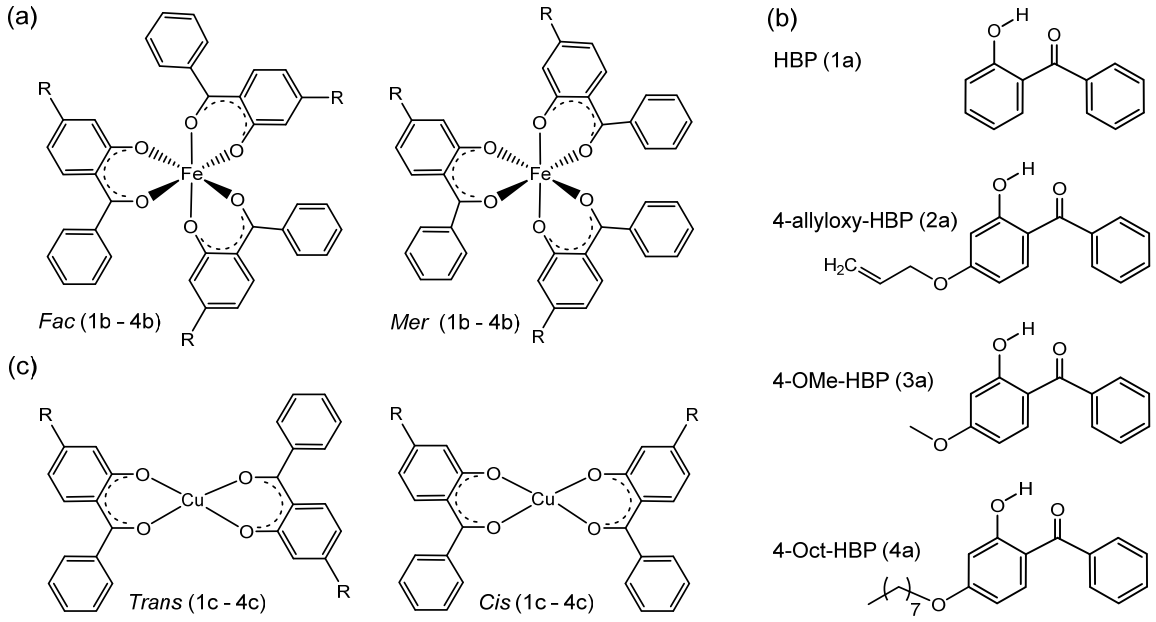

Scheme 1. Structure of the (a) *fac* and *mer* isomers of the four tris(2-hydroxybenzophenone)iron(III) complexes (**1b**) – (**4b**) in this study, containing the ligands (**1a**) – (**4a**) respectively. (b) Ligands 2-hydroxybenzophenone (ligand **1a** with R=H, abbreviated HBP), 2-hydroxy-4-(alloyloxy)benzophenone (ligand **2a** with R=OCH_2CHCH_2, abbreviated 4-alloyloxy-HBP), 2-hydroxy-4-methoxybenzophenone (ligand **3a** with R=OCH_3, abbreviated 4-OMe-HBP) and 2-hydroxy-4-(octyloxy)benzophenone (ligand **4a** with R=$O(CH_2)_7CH_3$, abbreviated 4-Oct-HBP). (c) *Trans* and *cis* isomers of the related bis(2-hydroxybenzophenone)copper(II) complexes (**1c**) – (**4c**) containing the same ligands (**1a**) – (**4a**) respectively.

2 Experimental

2.1 General

Melting points (m.p.) were determined with an Olympus BX51 system microscope, assembled on top of a Linkam THMS600 stage and connected to a Linkam TMS94 temperature programmer. UV/vis spectra were recorded on a Varian Cary 50 Conc ultra-violet/visible spectrophotometer. FTIR measurements (solid samples) were determined with a Bruker Tensor 27 IR spectrometer and Pike MIRacle ATR, running OPUS software (Version 1.1). MALDI-TOF-MS spectra (matrix assisted laser desorption/ionization time-of-flight mass spectrometry) were collected by a Bruker Microflex LRF20 in the negative reflection mode, using the minimum laser power required to observe signals.

2.2 Synthesis

The differently substituted 2-hydroxybenzophenone ligands needed for complexes (**1a**) – (**4a**) (see Scheme 1) were obtained from Sigma Aldrich and used as is. The *bis*(2-hydroxybenzophenone)copper(II) complexes (**1c**) – (**4c**) were synthesized and characterized as described in our previous publication [7].

The synthesis and characterization of *tris*(2-hydroxybenzophenone)iron(III) complexes (**1b**) and (**3b**) were previously reported. The published method was used to synthesize complexes (**1b**) – (**4b**) [3]. As example, the synthesis of the unsubstituted *tris*(2-hydroxybenzophenone)iron(III) (**1b**) is described.

From a reaction of $FeCl_3 \bullet 6H_2O$ (1 mmol) and NaSCN (3 mmol), a freshly made $Fe(SCN)_3$ solution was prepared. It was added dropwise to a stirred methanol solution of HBP ligand (**1a**) (3 mmol) in the presence of excess sodium methoxide (3 mmol) at room temperature. The color of the solution turned gradually darker and after 2 hours to dark red. The solution mixture was left at rest and a few days later dark red microcrystals of compound (**1b**) were formed. The microcrystals obtained were collected by filtration, washed with ethyl ether, dried in vacuo and recrystallized from dichloromethane.

2.2.1 Characterization data of $[Fe(2\text{-}HBP)_3]$ (**1b**)

Yield: 50%. Colour: Dark Red, M.p. 120ºC; IR $\bar{\upsilon}$ (cm^{-1}): 1597, 1557, 1329, 1240, 756, 698, 643 . UV: λ_{max} 325 nm, ε_{max} 3.80 $mol^{-1}dm^3cm^{-1}$ (DMF). MS Calcd. ($[M]^-$, negative mode): *m/z* 647.505. Found: *m/z* 647.566. Elemental analysis calculated for $FeC_{39}H_{27}O_6$ (element, %): C, 72.35; H, 4.20. obtained: C, 72.15; H, 4.33.

2.2.2 Characterization data of [Fe(4-allyloxy-HBP)$_3$] (**2b**)

Yield: 44%. Colour: Dark Red, M.p. 175ºC; IR $\bar{\upsilon}$ (cm^{-1}): 1550, 1498, 1243, 1165, 1114, 697. UV: λ_{max} 288 nm, ε_{max} 11.96 mol^{-1}dm^{3}cm^{-1} (DMF). MS Calcd. ([M]$^-$, negative mode): *m/z* 815.66. Found: *m/z* 815.226. Elemental analysis calculated for $FeC_{48}H_{39}O_9$ (element, %): C, 70.68; H, 4.82. obtained: C, 70.75; H, 4.31.

2.2.3 Characterization data of [Fe(4-OMe-HBP)$_3$] (**3b**)

Yield: 60%. Colour: Dark Red, M.p. 105ºC; IR $\bar{\upsilon}$ (cm^{-1}): 1549, 1504, 1244, 1213, 1163, 1114, 752. UV: λ_{max} 287 nm, ε_{max} 7.18 mol^{-1}dm^{3}cm^{-1} (DMF). MS Calcd. ([M]$^-$, negative mode): *m/z* 737.55. Found: *m/z* 737.519. Elemental analysis calculated for $FeC_{42}H_{33}O_9$ (element, %): C, 68.40; H, 4.51. obtained: C, 68.41; H, 4.64.

2.2.4 Characterization data of [Fe(4-Oct-HBP)$_3$] (**4b**)

Yield: 45%. Colour: Dark Red, M.p. 65ºC; IR $\bar{\upsilon}$ (cm^{-1}): 2954, 2854, 1501, 1226, 1117, 892, 840. UV: λ_{max} 289 nm, ε_{max} 8.25 mol^{-1}dm^{3}cm^{-1} (DMF). MS Calcd. ([M]$^-$, negative mode): *m/z* 1032.11. Found: *m/z* 1030.589. Elemental analysis calculated for $FeC_{63}H_{75}O_9$ (element, %): C, 73.31; H, 7.32. obtained: C, 72.96; H, 7.37.

2.3 Cyclic Voltammetry

Cyclic voltammetric (CV) measurements were done on a BAS100B Electrochemical Analyzer linked to a personal computer, utilizing the BAS100W Version 2.3 software. Measurements were done at 293 K and temperature was kept constant to within 0.5 K. A three-electrode cell was used, with a glassy carbon (surface area 0.0707 cm^2) working electrode, Pt auxiliary electrode and an Ag/AgCl (3M NaCl sat) reference electrode (BASI P/N MF-2052). The analyte was dissolved in DMF and separated from the reference electrode with a bridge filled with a 0.1 mol dm^{-3} tetra-n-butylammoniumhexafluorophosphate (TBAHFP) in DMF. The working electrode was polished on a Bühler polishing mat, first with 1 micron and then with ¼ micron diamond paste (in a figure-of-eight motion), rinsed with EtOH, H_2O and CH_3CN, and dried before each experiment. The electrochemistry measurements were performed on ca 0.002 mol dm^{-3} samples in solvent DMF for complex (**1b**) – (**4b**), containing 0.1 mol dm^{-3} tetrabutylammonium hexafluorophosphate TBAHFP, as supporting electrolyte. The voltammograms were obtained at room temperature under a blanket of argon. Scan rates were 0.020 – 10.240 V s^{-1}. Ferrocene (FcH) was used as an internal standard, and all cited potentials were referenced against the FcH/FcH$^+$ couple, as suggested by IUPAC [9]. E_{pa} = anodic peak potential and i_{pa} = anodic peak current, E_{pc} = cathodic peak potential and i_{pc} = cathodic peak current. The reduction potential is determined by the mean of the oxidation and reduction potential

$E_{1/2}$ = (E_{pa} – E_{pc})/2, the peak current voltage separation $\Delta E_p = E_{pa} - E_{pc}$. $E^{o'}$ (FcH/FcH^+) = 0.66(5) V *vs* SHE in [^{n}(Bu_4)N][PF_6]/CH_3CN [10], and thus 0.416 V *vs* SCE (Saturated calomel (SCE) = 0.2444 V *vs* SHE).

2.4 DFT calculations

Density functional theory (DFT) calculations were performed on the neutral molecules using B3LYP which is composed of the Becke 88 exchange functional [11] in combination with the LYP correlation functional [12], as implemented in the Gaussian 16 package [13]. The triple-ζ 6-311G(d,p) basis set was used for lighter atoms (C, H, O) and the def2-TZVPP basis set [14] for both the core and valence electrons of Fe. Calculations were performed in the gas phase and also in DMF as implicit solvent. The solvation model used is IEF-PCM, the polarizable continuum model (PCM) [15] that applies the integral equation formalism variant (IEF-PCM) [16]. The input coordinates for the compounds were constructed using Chemcraft [17].

3 Results and Discussion

3.1 Synthesis

The iron(III) complexes (**1b**) – (**4b**), containing a variety of 2-hydroxybenzophenone ligands, were prepared, using the method reported in literature [7] (see Scheme 2). The synthesis required the stirring of 3 eq. of the respective 2-hydroxybenzophenone ligand and 1 eq. $Fe(SCN)_3$ (prepared from $FeCl_3 \cdot 6H_2O$ and NaSCN) in a methanol solution in the presence of excess sodium methoxide. The resulting dark-red precipitates were isolated by filtration, washed with ethyl ether, vacuum-dried and recrystallized in dichloromethane. The complexes, of the formula [Fe(ligand)$_3$] are stable in air and insoluble in water, slightly soluble in dimethyl sulfoxide and dichloromethane and most soluble in dimethylformamide.

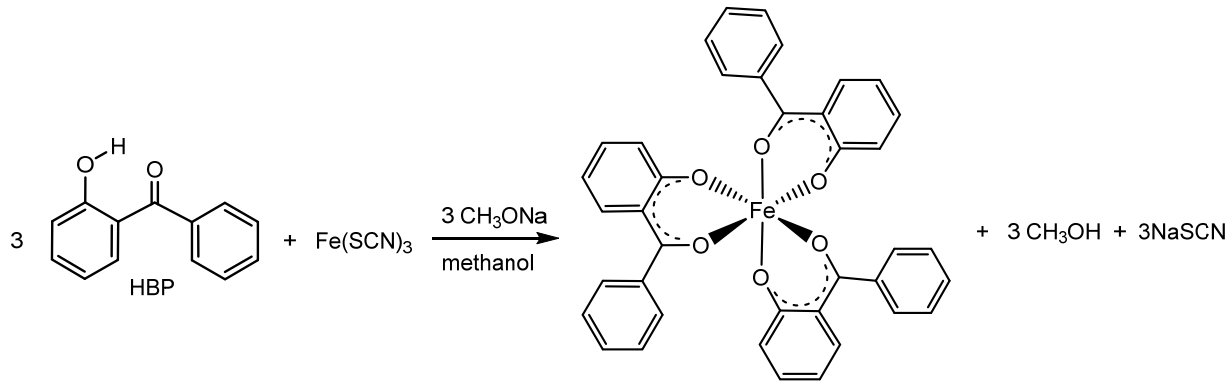

Scheme 2. Synthesis route for preparing *tris*(2-hydroxybenzophenone)iron(III) complex (**1b**) from ligand HBP (**1a**).

3.2 DFT results

DFT calculations have been done to get more information on the geometry, spin state and electronic structure of the [Fe(2-hydroxybenzophenone)$_3$] complexes of this study.

3.2.1 Spin state

Since each ligand undergoes only one deprotonation upon coordination to Fe, all mononuclear iron(III) complexes are neutral. The oxidation state of the metal is 3+ and therefore the neutral [Fe(2-hydroxybenzophenone)$_3$] complexes have 5 d electrons. DFT calculations showed that the complexes are high spin (see the energies in **Table 1**) with electron occupation $d^1_{xy}d^1_{xz}d^1_{yz}d^1_{x^2-y^2}d^1_{z^2}$. This result agrees with the experimental and calculated spin state of tris(β-diketonato)iron(III) complexes, that have many structural similarities to the tris(2-hydroxybenzophenone)iron(III) complexes of this study. The tris(β-diketonato)iron(III) complexes are also octahedral, containing three bidentate ligands that each forms a six-membered ring with Fe, and are coordinated through oxygen atoms to iron(III) [18–20]. The high-spin DFT results for [Fe(2-hydroxybenzophenone)$_3$] also agree with experimental magnetic susceptibility results reported on an iron(III) complex containing 2,4-dihydroxy-benzophenone-S-methyl-thiosemicarbazone, that were consistent with a high-spin d^5 iron centre [21][22]. Optimization of the different spin states of the anion, tris(2-hydroxybenzophenone)iron(II) with charge 1-, shows that [Fe(2-hydroxybenzophenone)$_3$]$^-$ is high spin (S = 2), see the energies in Table 1.

Table 1. Relative gas phase energies for different spin states for both *fac* and *mer* geometries of the *tris*(2-hydroxybenzophenone)iron(III), complex (**1b**), and the reduced *tris*(2-hydroxybenzophenone)iron(II) anion, calculated by DFT.

Complex	Multiplicity	Spin state		Relative E (eV)			
				B3LYP[a]	M06[a]	OPBE0[b]	OLYP[b]
Neutral	2	1/2	*fac*	0.61	1.60	1.58	0.58
	4	3/2	*fac*	0.73	-	1.24	0.68
	6	5/2	*fac*	0.00	0.00	0.00	0.00
	2	1/2	*mer*	0.58	1.60	1.54	0.51
	4	3/2	*mer*	0.64	1.39	1.25	0.57
	6	5/2	*mer*	0.04	0.12	0.06	0.05
Reduced	1	0	*fac*	0.79	1.47	1.62	0.50

3	1	*fac*	1.00	1.40	1.52	0.72
5	2	*fac*	0.01	0.00	0.00	0.00
1	0	*mer*	0.79	1.55	1.61	0.52
3	1	*mer*	0.92	1.45	1.42	0.71
5	2	*mer*	0.00	0.15	0.11	0.00

a Gaussian with B3LYP [11,12,23] or M06 [24] functionals and basis 6-311G(d,p)/def2-TZVPP
b ADF OPBE0 [25] and OLYP [12,26] functionals and basis TZ2P

3.2.2 Geometry

The Fe (III) atom is chelated by three 2-hydroxybenzopheone ligands via the phenolate and carbonyl oxygen atoms. Both oxygen atoms of each 2-hydroxybenzophenone ligand bind to the metal to form three six-membered chelate rings round the metal ion to give an octahedral structure as shown in **Scheme 1**. Two isomers are possible for the [Fe(2-hydroxybenzophenone)$_3$] complexes containing the unsymmetrically 2-hydroxybenzophenone ligands: a facial isomer (*fac*), where the three ligands are symmetrically arranged around the metal core, and a meridional isomer (*mer*), see Scheme 1. The *fac* and *mer* isomers of the four substituted [Fe(2-hydroxybenzophenone)$_3$] complexes (**1b**) – (**4b**) were optimized by DFT calculations without any symmetry constraint.

The *fac* isomers are the preferred orientation for complexes **(1b)** and **(3b)**, observed to be slightly more stable (ca 0.04 eV lower in energy in gas phase) than the *mer* isomers as shown in **Table 2**. No experimental crystal structures of *tris*(2-hydroxybenzophenone)iron(III) could be found, only of the related *fac* tris(2-(1-oxopropyl)phenolato)iron(III) (CSD reference YUHXEF [3]). Statistical the *mer* : *fac* ratio is 3:1 [27]. The *mer* isomer is also preferred on ground of steric effects when the ligands contain large substituent groups near the coordination centre [28,29]. For complexes **(2b)** and **(4b)**, containing larger 4-substituents, the *mer* isomers were lower in energy and therefore the preferred orientation. Though, according to the Boltzmann probability distribution, both isomers should be present in an experimental sample of the complex, see **Table 2**.

Table 2. B3LYP/6-311G(d,p)/def2-TZVPP calculated relative energies and population of the *tris*(2-hydroxybenzophenone)iron(III) complexes 1 – 4 from this study.

No	**complex**	**ΔE[a] (eV) gas phase**	**ΔE[a] (eV) DMF**	**ΔG[a] (eV) DMF**	**% *fac*[b]**	**% *mer*[b]**
1b	Fe(HBP)$_3$	-0.04	-0.04	-0.04	84.3	15.7
2b	Fe(4-allyloxy)$_3$	0.05	0.06	0.06	10.3	89.7
3b	Fe(4-OMe)$_3$	-0.04	-0.03	-0.03	75.8	24.2
4b	Fe(4-Oct)$_3$	0.11	0.08	0.15	0.2	99.8

a *fac* relative to *mer*; thus if ΔE < 0, *fac* more stable, ΔE > 0, *mer* more stable

b Calculated from free energies in DMF, using the Boltzmann equation.

3.2.3 Electronic structure

A change in the ligand structure during the formation of the iron(III) complexes enables the formation of new bonds between the ligands and metal ion. To determine the most reactive sites in the newly formed molecule, the energy of the frontier molecular orbitals (FMOs) is calculated. DFT calculations also allow determination of FMO loci in order to correctly allocate the observed electrochemical phenomena.

HOMOs (highest occupied molecular orbitals) and LUMOs (lowest unoccupied molecular orbitals), play an important role in reduction and oxidation reactions, since reduction and oxidation involve the addition or removal of an electron to or from a FMO of the species. Evaluation of the FMOs of the [Fe(HBP)$_3$] complex, Figure 1, showed that the top three LUMOs of [Fe(HBP)$_3$], **(1b)** are mainly on Fe and the top three HOMOs are mainly distributed over the ligands. Reduction, addition of an electron into the LUMO of the complex, thus occurs around the Fe metal. The lowest energy electronic UV-vis excitation will all be of ligand to metal charge transfer (LMCT), involving excitation of an electron from a ligand-based HOMO to a metal based LUMO.

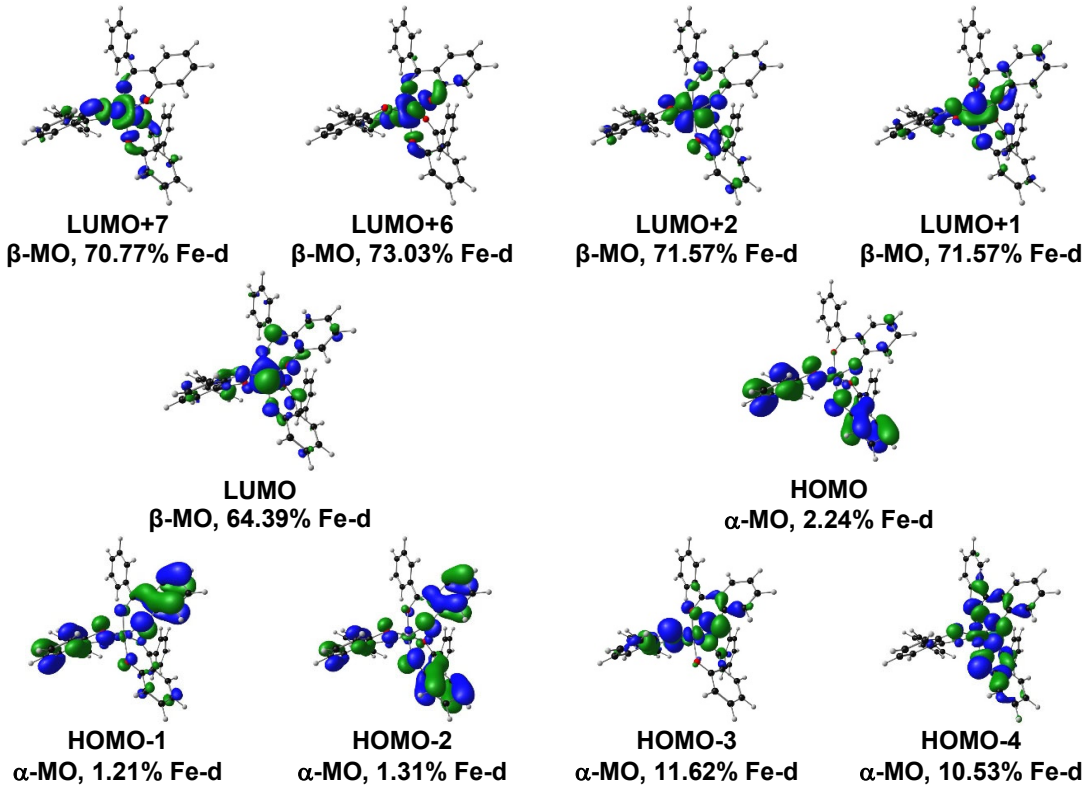

Figure 1. Selected DFT calculated Kohn−Sham frontier MO plots of the B3LYP/6-311G(d,p)/def2-TZVPP gas phase optimized geometry of *fac* [Fe(2-hydroxybenzophenone)$_3$], complex (**1b**). A contour of 0.05 e/Å^3 was used for the orbital plot. Colour code of atoms (online version): Fe (orange), C (black), O (red), H (grey).

Reduction of [Fe^{III}(2-hydroxybenzophenone)$_3$] leads to [Fe^{II}(2-hydroxybenzophenone)$_3$]$^-$, since the reduction is iron based. Further reductions will involve the LUMOs of Fe^{II}(2-hydroxybenzophenone)$_3$]$^-$. Since rearrangement of the frontier MOs sometimes occur during reduction [30], the LUMO of the reduced molecule needs to be considered when assigning the locus of the follow-up reduction. In Figure 2 the HOMO and the top three LUMOs of Fe^{II}(2-hydroxybenzophenone)$_3$]$^-$ is shown. The HOMO of Fe^{II}(2-hydroxybenzophenone)$_3$]$^-$ is iron based and of the same character as the LUMO (a β MO) of [Fe^{III}(2-hydroxybenzophenone)$_3$], where the electron was added upon reduction. LUMO+16 of Fe^{II}(2-hydroxybenzophenone)$_3$]$^-$ is the first iron based unoccupied MO. The top LUMOs are all ligand based. Reduction of Fe^{II}(2-hydroxybenzophenone)$_3$]$^-$ will thus be ligand based. The calculated Mulliken spin density of Fe for *fac* [Fe^{III}(2-hydroxybenzophenone)$_3$] and *fac* Fe^{II}(2-hydroxybenzophenone)$_3$]$^-$ are 4.203 and 3.826 respectively, consistent with metal-based reduction.

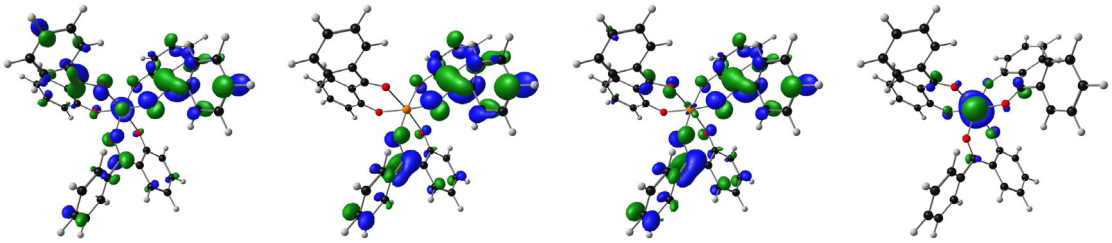

Figure 2. Selected DFT calculated Kohn−Sham frontier MO plots of the B3LYP/6-311G(d,p)/def2-TZVPP gas phase optimized geometry of the reduced *fac* [Fe(2-hydroxybenzophenone)$_3$], complex (**1b**) with charge 1-. A contour of 0.04 e/Å^3 was used for the orbital plot. Colour code of atoms (online version): Fe (orange), C (black), O (red), H (grey).

3.3 CV results

Here we present the redox behaviour of tris(2-hydroxybenzophenone)iron(III) complexes (**1b**) – (**4b**) in **Figure 3** at indicated scan rates using cyclic voltammetry (CV) measurements in DMF

solvent media, with the results summarized in **Table 3**. The CVs of the free, uncoordinated ligands (**1a**), (**3a**) and (**4a**) were previously reported in DMF [31], while the CVs of bis(2-hydroxybenzophenone)copper(II) complexes (**1c**) – (**4c**) were previously reported in DMSO [7]. The CVs of ligand (**2a**) and bis(2-hydroxybenzophenone)copper(II) complexes (**1c**) – (**4c**) are thus also reported in DMF in this study, to be compared to the CVs of the tris(2-hydroxybenzophenone)iron(III) complexes (**1b**) – (**4b**) in the same solvent, DMF.

For each of *tris*(2-hydroxybenzophenone)iron(III) complex (**1b**) – (**4b**), a reduction peak at ca -1 V *versus* FcH/FcH^+ was recorded. The DFT studies showed that this first reduction peak is Fe-based. For each complex, another slightly broader (peak current voltage separation > 0.09 V) reduction peak at ca -2 V *versus* FcH/FcH^+, slightly lower than the reduction of the free ligand, is also observed, see **Figure 5** for (**3b**) as example. The peak cathodic current of the second reduction peak is ca 3 x that of the first reduction peak. The DFT studies showed that the second reduction peak is ligand-based. The second observed reduction is thus suggested to be the near simultaneous reduction of the three coordinated ligands.

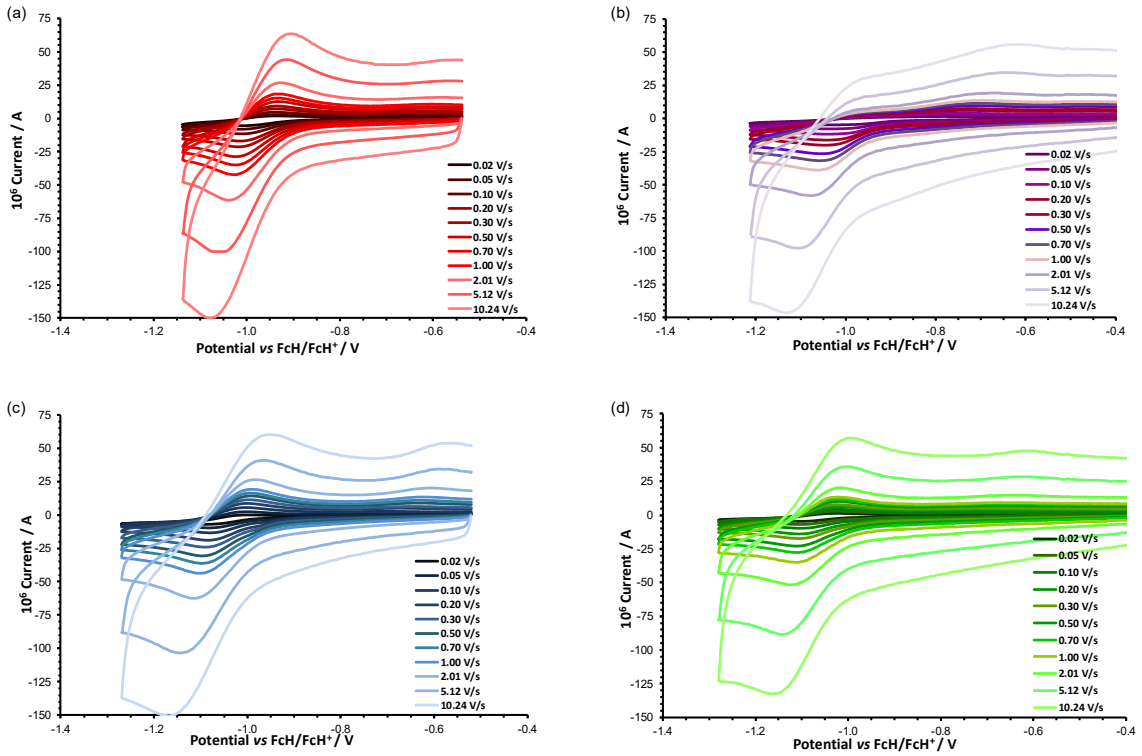

Figure 3. Cyclic voltammograms (*versus* FcH/FcH^+) of the reduction of 0.002 mol dm^{-3} DMF solution of (a) $[Fe(2\text{-}HBP)_3]$ (**1b**), (b) $[Fe(4\text{-allyloxy-}HBP)_2]$ (**2b**), (c) $[Fe(4\text{-}OMe)_3]$ (**3b**) and (d) $[Fe(4\text{-}Oct)_3]$ (**4b**) at the indicated scan rates. All CVs scanned in the negative direction from ca -0.4 V.

From Figure 3 we observe that the Fe^{III}/Fe^{II} redox process is electrochemically reversible for complexes (**1b**), (**3b**) and (**4b**), due to a very small peak separation, $\Delta E_p = E_{pa} - E_{pc}$, of ca 0.07 V, but chemically quasi reversible to irreversible due to peak current ratios < 1. The peak reduction current is directly proportional to the square root of the scan rate according to the Randles–Ševčík equation, showing that the reduction process is diffusion controlled [32], see **Figure 4**. The same electrochemical behaviour was obtained at all scan rates 0.020 – 10.240 V s^{-1}. Varying redox potentials for complexes (**1b**) – (**4b**) in **Table 3** are ascribed to different electron densities at the Fe centre as a result of the electronic character of different substituents on the 2-hydroxybenzophenone ligands. The molecules with electron donating group(s) (namely (**2b**) – (**4b**)) result into more negative reduction potentials because of the electron donation from the alkoxy substituents. The effect of an aromatic R group on the reduction potential of a molecule is an interplay of the inductive effect through the σ-system and a resonance effect through the π-system. A *para*-alkoxy substituent on benzophenone led to a less negative redox potential as expected if only the induction effect was present (for example, E_{pc}(4-Me-benzophenone) = −2.275 and E_{pc}(4-OMe-benzophenone) = −2.236) [33]. A *para*-alkoxy substituent on 2-hydroxybenzophenone seems also to have a less negative redox potential, as expected, if only the induction effect was present, since in all relationships involving E_{pc}, the data points for 4-alkoxy-benzophenone molecules lay above the linear line at a less negative redox potential [34]. This might explain the relative small shift of 0.01 – 0.10 V in the reduction potential of the alkoxy-containing ligands (**2a**) – (**4a**), complexes (**2b**) – (**4b**) and (**2c**) – (**4c**), relative to the 2-hydroxybenzophenone (**1a**), the iron(III) complex (**2a**) and the copper(II) (**3a**) respectively, see **Figure 6** and the data in **Table 3**. The iron-based reduction of the *tris*(2-hydroxybenzophenone)Fe(III) complexes (**1b**) – (**4b**) occurs at a potential more than 1 V more positive than the reduction of the respective free ligands (**1a**) – (**4a**), similarly as was found for the copper-based reduction of *bis*(2-hydroxybenzophenone)copper(II) complexes (**1c**) – (**4c**) in DMF (this study) and in DMSO [7].

The shifts in the experimental reduction potentials for complexes containing electron donating *versus* unsubstituted ligand, shows there is good communication between the different substituents and the rest of the Fe complex. We could not find any report with cyclic voltammetry data in literature on the iron(III) complexes of this study, though the obtained iron(III/II) reduction potential for (**1b**) – (**4b**) is in the same region as measured for the structurally related tris(β-diketonato)iron(III) complexes where the β-diketonato is electron donating. For example for β-diketonate = acetylacetone (-1.038 V *versus* FcH/FcH^+), 1-benzoylacetone (-0.971 V *versus* FcH/FcH^+) and 1,3-dibenzoylacetone (-0.921 V *versus* FcH/FcH^+) [18].

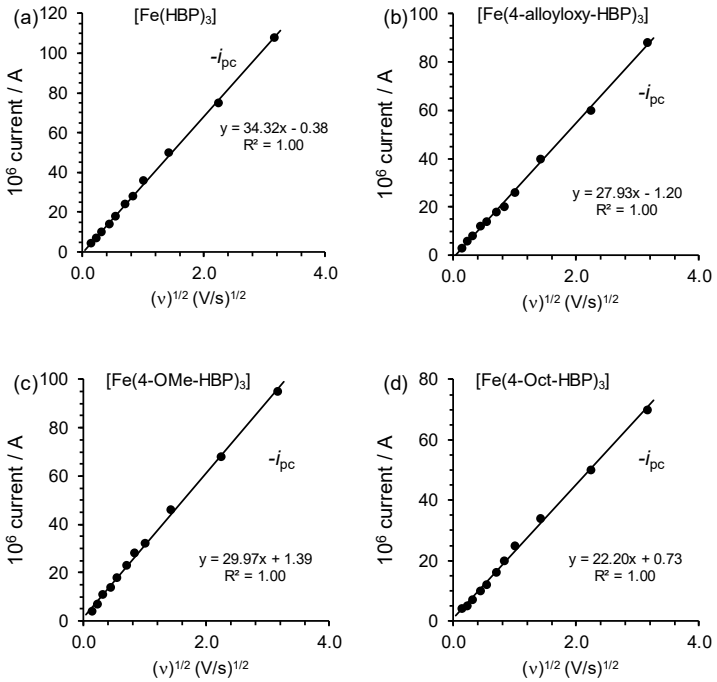

Figure 4. Relationship between peak reduction current and the square root of the scan rate according to the Randles–Ševčík equation (a) [Fe(2-HBP)$_3$] (**1b**), (b) [Fe(4-allyloxy-HBP)$_2$] (**2b**), (c) [Fe(4-OMe)$_3$] (**3b**) and (d) [Fe(4-Oct)$_3$] (**4b**).

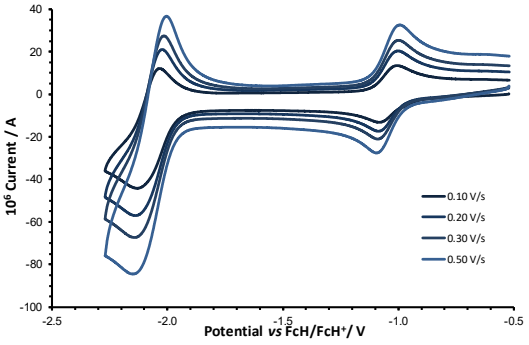

Figure 5. Cyclic voltammograms (*versus* FcH/FcH$^+$) of 0.002 mol dm^{-3} DMF solution of [Fe(4-OMe)$_3$] (**3b**) at the indicated scan rates.

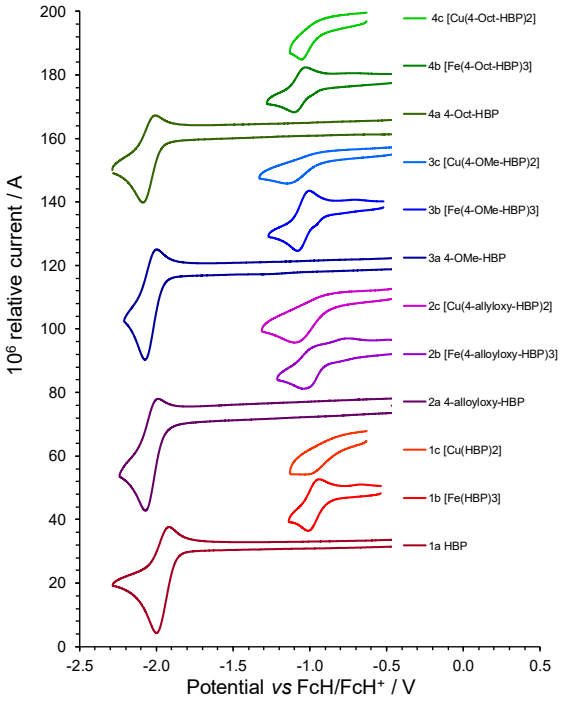

Figure 6. Cyclic voltammograms (*versus* FcH/FcH^+) of ligands (**1a**) – (**4a**), tris(2-hydroxybenzophenone)iron(III) complexes (**1b**) – (**4b**) and bis(2-hydroxybenzophenone)copper(II) complexes (**1c**) – (**4c**) at a scan rate of 0.100 V s^{-1} in DMF as solvent and TBAHFP as supporting electrolyte. Copper complex (**1c**) was poorly soluble in DMF.

Table 3. Electrochemical data (E *versus* FcH/FcH^+ in DMF as solvent, I in A, for 0.100 V s^{-1} scan) of tris(2-hydroxybenzophenone)iron(III) complexes, bis(2-hydroxybenzophenone)copper(II) complexes and the ligands.

No	Complex/ligand	E_{pc}	E_{pa}	$E_{1/2}$	ΔE	I_{pa}/I_{pc}
1b	$[Fe(2\text{-}HBP)_3]$	-1.006	-0.937	-0.972	0.069	0.30
2b	$[Fe(4\text{-allyloxy})_3]$	-1.030	-	-	-	-
3b	$[Fe(4\text{-}OMe)_3]$	-1.078	-1.004	-1.041	0.074	0.73
4b	$[Fe(4\text{-}Oct)_3]$	-1.098	-1.026	-1.062	0.072	0.71
1c	$[Cu(2\text{-}HBP)_2]$	-1.023	-	-	-	-
2c	$[Cu(4\text{-allyloxy})_2]$	-1.029	-	-	-	-
3c	$[Cu(4\text{-}OMe)_2]$	-1.134	-	-	-	-
4c	$[Cu(4\text{-}Oct)_2]$	-1.037	-	-	-	-
1a	2-HBP[a]	-1.997	-1.914	-1.955	0.083	0.21
2a	4-allyloxy[a]	-2.067	-1.974	-2.021	0.093	0.31
3a	4-OMe [a]	-2.080	-2.000	-2.040	0.079	0.20
4a	4-Oct[a]	-2.087	-2.008	-2.048	0.079	0.18

a Data from this study (**2a**) and from reference [31] (**1a**), (**3a**) and (**4a**).

4 Conclusions

For tris(2-hydroxybenzophenone)iron(III) complexes the experimental $Fe^{III/II}$ reduction was observed at ca -1 V *versus* FcH/FcH^+, followed by a second (ligand based) reduction at ca -2 V *versus* FcH/FcH^+. The ligand based peak reduction peak is ca three times that of the first reduction peak, suggesting a near simultaneous reduction of the three coordinated ligands. Complexes with electron donating group(s) result in more negative reduction potentials because of the electron donating alkoxy substituents. The shifts in experimental reduction potentials show there is good communication between the different substituents and the central iron(II) ion. Computational chemistry analyses contributed in the assessment of experimental results. An electronic structure analysis shows that the top three LUMOs of the complexes are mainly on Fe and the top three HOMOs are distributed over the ligands. DFT calculations showed that [Fe(2-hydroxybenzophenone)$_3$] complexes are high-spin. Calculations further showed that both the *fac* and *mer* isomers tris(2-hydroxybenzophenone)iron(III) complexes, can exist.

Acknowledgements

The authors are grateful to acknowledge the Central Research Fund of University of the Free State, the Sasol University Collaboration Programme and the National Research Foundation (NRF) in South Africa for financial support (Grant Nos: 129270 (JC) and 132504 (JC)). The High-Performance Computing facility of the UFS, the CHPC of South Africa (Grant no CHEM0947) and the Norwegian Supercomputing Program (Sigma2, Grant No. NN9684K) are acknowledged for computer time.

Declaration of Competing Interest

The authors declare that they have no known competing financial interests or personal relationships that could have appeared to influence the work reported in this paper.

Ethics Statement

This work does not require any ethical statement.

Credit author statement

EC: Investigation, Validation, Formal analysis, Data curation, Methodology, Writing- Reviewing and Editing.

EHGL: Resources, Reviewing and Editing

JC: Conceptualization, Supervision, Resources, Validation, Methodology, Funding acquisition, Project administration, Writing- Reviewing and Editing.

Supporting Information

Optimized coordinates of the DFT calculations.

References

[1] M. Prejanò, M.E. Alberto, N. Russo, M. Toscano, T. Marino, The Effects of the Metal Ion Substitution into the Active Site of Metalloenzymes: A Theoretical Insight on Some Selected Cases, Catalysts. 10 (2020) 1038. https://doi.org/10.3390/catal10091038.

[2] P.B. Pansuriya, M.N. Patel, Iron(III) complexes: Preparation, characterization, antibacterial activity and DNA-binding, J. Enzyme Inhib. Med. Chem. 23 (2008) 230–239. https://doi.org/10.1080/14756360701474657.

[3] M. Lalia-Kantouri, T. Dimitriadis, C.D. Papadopoulos, M. Gdaniec, A. Czapik, A.G. Hatzidimitriou, Synthesis and Structural Characterization of Iron(III) Complexes with 2-Hydroxyphenones, Zeitschrift Für Anorg. Und Allg. Chemie. 635 (2009) 2185–2190. https://doi.org/10.1002/zaac.200900016.

[4] B. İlhan Ceylan, A. Yilmaz, O. Bölükbaşı, E.T. Acar, M. Özyürek, Y. Kurt, B. Ülküseven, A square-pyramidal iron(III) complex obtained from 2-hydroxy-benzophenone- S -allyl-thiosemicarbazone: synthesis, characterization, electrochemistry, quantum chemical studies and antioxidant capability, J. Coord. Chem. 73 (2020) 120–136. https://doi.org/10.1080/00958972.2020.1715372.

[5] R. Esposito, U. Raucci, M.E. Cucciolito, R. Di Guida, C. Scamardella, N. Rega, F. Ruffo, Iron(III) Complexes for Highly Efficient and Sustainable Ketalization of Glycerol: A Combined Experimental and Theoretical Study, ACS Omega. 4 (2019) 688–698. https://doi.org/10.1021/acsomega.8b02546.

[6] K. Rydel-Ciszek, T. Pacześniak, I. Zaborniak, P. Błoniarz, K. Surmacz, A. Sobkowiak, P. Chmielarz, Iron-Based Catalytically Active Complexes in Preparation of Functional

Materials, Processes. 8 (2020) 1683. https://doi.org/10.3390/pr8121683.

[7] E. Chiyindiko, E.H.G. Langner, J. Conradie, Electrochemical behaviour of copper(II) complexes containing 2-hydroxyphenones, Electrochim. Acta. 424 (2022) 140629. https://doi.org/10.1016/j.electacta.2022.140629.

[8] A.A. Adeniyi, J. Conradie, Cyclic Voltammetric and DFT Analysis of the Reduction of Manganese(III) Complexes with 2-Hydroxybenzophenones, Electroanalysis. 32 (2020) 2913–2925. https://doi.org/10.1002/elan.202060362.

[9] G. Gritzner, J. Kuta, Recommendations on reporting electrode potentials in nonaqueous solvents (Recommendations 1983), Pure Appl. Chem. 56 (1984) 461–466. https://doi.org/10.1351/pac198456040461.

[10] A.J.L. Pombeiro, Electron-donor/acceptor properties of carbynes, carbenes, vinylidenes, allenylidenes and alkynyls as measured by electrochemical ligand parameters, J. Organomet. Chem. 690 (2005) 6021–6040. https://doi.org/10.1016/j.jorganchem.2005.07.111.

[11] A.D. Becke, Density-functional exchange-energy approximation with correct asymptotic behavior, Phys. Rev. A. 38 (1988) 3098–3100. https://doi.org/10.1103/PhysRevA.38.3098.

[12] C. Lee, W. Yang, R.G. Parr, Development of the Colle-Salvetti correlation-energy formula into a functional of the electron density, Phys. Rev. B. 37 (1988) 785–789. https://doi.org/10.1103/PhysRevB.37.785.

[13] M.J. Frisch, G.W. Trucks, H.B. Schlegel, G.E. Scuseria, M.A. Robb, J.R. Cheeseman, G. Scalmani, V. Barone, G.A. Petersson, H. Nakatsuji, X. Li, M. Caricato, A. V. Marenich, J. Bloino, B.G. Janesko, R. Gomperts, B. Mennucci, H.P. Hratchian, J. V. Ortiz, A.F. Izmaylov, J.L. Sonnenberg, D. Williams-Young, F. Ding, F. Lipparini, F. Egidi, J. Goings, B. Peng, A. Petrone, T. Henderson, D. Ranasinghe, V.G. Zakrzewski, J. Gao, N. Rega, G. Zheng, W. Liang, M. Hada, M. Ehara, K. Toyota, R. Fukuda, J. Hasegawa, M. Ishida, T. Nakajima, Y. Honda, O. Kitao, H. Nakai, T. Vreven, K. Throssell, J. Montgomery, J. A., J.E. Peralta, F. Ogliaro, M.J. Bearpark, J.J. Heyd, E.N. Brothers, K.N. Kudin, V.N. Staroverov, T.A. Keith, R. Kobayashi, J. Normand, K. Raghavachari, A.P. Rendell, J.C. Burant, S.S. Iyengar, J. Tomasi, M. Cossi, J.M. Millam, M. Klene, C. Adamo, R. Cammi, J.W. Ochterski, R.L. Martin, K. Morokuma, O. Farkas, J.B. Foresman, D.J. Fox, Gaussian 16, Revision B.01, (2016).

[14] F. Weigend, R. Ahlrichs, Balanced basis sets of split valence, triple zeta valence and quadruple zeta valence quality for H to Rn: Design and assessment of accuracy, Phys. Chem. Chem. Phys. 7 (2005) 3297. https://doi.org/10.1039/b508541a.

[15] A. V. Marenich, C.J. Cramer, D.G. Truhlar, Universal Solvation Model Based on Solute Electron Density and on a Continuum Model of the Solvent Defined by the Bulk Dielectric Constant and Atomic Surface Tensions, J. Phys. Chem. B. 113 (2009) 6378–6396. https://doi.org/10.1021/jp810292n.

[16] R.E. Skyner, J.L. Mcdonagh, C.R. Groom, T. Van Mourik, A review of methods for the calculation of solution free energies and the modelling of systems in solution, Phys. Chem. Chem. Phys. 17 (2015) 6174–6191. https://doi.org/10.1039/C5CP00288E.

[17] Chemcraft - graphical software for visualization of quantum chemistry computations., (n.d.). http://www.chemcraftprog.com/.

[18] M.M. Conradie, J. Conradie, Electrochemical behaviour of Tris(β-diketonato)iron(III) complexes: A DFT and experimental study, Electrochim. Acta. 152 (2015) 512–519. https://doi.org/10.1016/j.electacta.2014.11.128.

[19] M.M. Conradie, P.H. van Rooyen, J. Conradie, Crystal and electronic structures of tris[4,4,4-Trifluoro-1-(2-X)-1,3-butanedionato]iron(III) isomers (X=thienyl or furyl): An X-ray and computational study, J. Mol. Struct. 1053 (2013) 134–140. https://doi.org/10.1016/j.molstruc.2013.09.014.

[20] I. Diaz-Acosta, J. Baker, W. Cordes, P. Pulay, Calculated and Experimental Geometries and Infrared Spectra of Metal Tris-Acetylacetonates: Vibrational Spectroscopy as a Probe of Molecular Structure for Ionic Complexes. Part I, J. Phys. Chem. A. 105 (2001) 238–244. https://doi.org/10.1021/jp0028599.

[21] Y.D. Kurt, B. Ülküseven, S. Tuna, M. Ergüven, S. Solakoğlu, Iron(III) and nickel(II) template complexes derived from benzophenone thiosemicarbazones, J. Coord. Chem. 62 (2009) 2172–2181. https://doi.org/10.1080/00958970902787775.

[22] Y. Kurt, A. Koca, M. Akkurt, B. Ülküseven, Iron(III) and nickel(II) complexes of O,N,N,O-chelating benzophenone thiosemicarbazone: Electrochemistry and in situ spectroelectrochemistry, Inorganica Chim. Acta. 388 (2012) 148–156. https://doi.org/10.1016/j.ica.2012.03.023.

[23] B. Miehlich, A. Savin, H. Stoll, H. Preuss, Results obtained with the correlation energy density functionals of Becke and Lee, Yang and Parr, Chem. Phys. Lett. 157 (1989) 200–206. https://doi.org/10.1016/0009-2614(89)87234-3.

[24] Y. Zhao, D.G. Truhlar, The M06 suite of density functionals for main group thermochemistry, thermochemical kinetics, noncovalent interactions, excited states, and transition elements: two new functionals and systematic testing of four M06-class functionals

and 12 other function, Theor. Chem. Acc. 120 (2008) 215–241. https://doi.org/10.1007/s00214-007-0310-x.

[25] M. Swart, A.W. Ehlers, K. Lammertsma, Performance of the OPBE exchange-correlation functional, Mol. Phys. 102 (2004) 2467–2474. https://doi.org/10.1080/00268970420002750l7.

[26] N.C. Handy, A.J. Cohen, Left-right correlation energy, Mol. Phys. 99 (2001) 403–412. https://doi.org/10.1080/00268970010018431.

[27] R. Gostynski, J. Conradie, E. Erasmus, Significance of the electron-density of molecular fragments on the properties of manganese(III) β-diketonato complexes: an XPS and DFT study, RSC Adv. 7 (2017) 27718–27728. https://doi.org/10.1039/C7RA04921H.

[28] J. Conradie, Bond stretch isomers of d4 tris(benzoylacetonato-κ2O,O')Mn(III), Comput. Theor. Chem. 1087 (2016) 1–5. https://doi.org/10.1016/j.comptc.2016.04.022.

[29] T.L. Ngake, J.H. Potgieter, J. Conradie, Tris(β-ketoiminato)ruthenium(III) complexes: Electrochemical and computational chemistry study, Electrochim. Acta. 320 (2019) 134635. https://doi.org/10.1016/j.electacta.2019.134635.

[30] J. Ferrando-Soria, O. Fabelo, M. Castellano, J. Cano, S. Fordham, H.C. Zhou, Multielectron oxidation in a ferromagnetically coupled dinickel(II) triple mesocate, Chem. Commun. 51 (2015) 13381–13384. https://doi.org/10.1039/c5cc03544a.

[31] A.A. Adeniyi, T.L. Ngake, J. Conradie, Cyclic Voltammetric Study of 2-Hydroxybenzophenone (HBP) Derivatives and the Correspondent Change in the Orbital Energy Levels in Different Solvents, Electroanalysis. 32 (2020) 2659–2668. https://doi.org/10.1002/elan.202060163.

[32] N. Elgrishi, K.J. Rountree, B.D. McCarthy, E.S. Rountree, T.T. Eisenhart, J.L. Dempsey, A Practical Beginner's Guide to Cyclic Voltammetry, J. Chem. Educ. 95 (2018) 197–206. https://doi.org/10.1021/acs.jchemed.7b00361.

[33] E. Chiyindiko, E.H.G. Langner, J. Conradie, Electrochemical behaviour of 2-hydroxybenzophenones and related molecules, Results Chem. 4 (2022) 100332. https://doi.org/10.1016/j.rechem.2022.100332.

[34] E. Chiyindiko, J. Conradie, An electrochemical and computational chemistry study of substituted benzophenones, Electrochim. Acta. 373 (2021) 137894. https://doi.org/10.1016/j.electacta.2021.137894.